RJC

RASĀYAN *J. Chem.*
Vol. 11 | No. 3 |1244 - 1254 | July - September | 2018
ISSN: 0974-1496 | e-ISSN: 0976-0083 | CODEN: RJCABP
http://www.rasayanjournal.com
http://www.rasayanjournal.co.in

EFFECT OF Ti^{4+}/CLAY RATIO ON THE PROPERTIES OF TITANIUM PILLARED BENTONITE AND ITS APPLICATION FOR Cr (VI) REMOVAL

Tarmizi Taher[1], Risfidian Mohadi[2] and Aldes Lesbani[1,2,*]

[1]Department of environmental sciences, Graduate School of Universitas Sriwijaya, Jl. Padang Selasa, No. 524, Bukit Besar, Palembang, Indonesia

[2]Department of Chemistry, Faculty of Mathematics and Natural Sciences, Universitas Sriwijaya, Jl. Palembang-Prabumulih, Km. 32, Ogan Ilir, South Sumatera, Indonesia

*E-mail: aldeslesbani@pps.unsri.ac.id

ABSTRACT

Natural abundant bentonite collected from Jambi Province, Indonesia has been successfully pillared with titanium by using titanium propoxide as the titanium source. The titanium pillared bentonite (Ti-PilB) was prepared with different Ti^{4+}/clay ratios ranging from 1 to 15 mmol/g in order to evaluate the maximum amount of the titanium pillar in the interlayer space of bentonite. The natural bentonite (NB) and Ti-PilB were characterized using X-ray Diffraction (XRD), Fourier Transform Infrared Spectroscopy (FTIR), and X-ray Fluorescence (XRF). The Ti-PilB sample was used as an adsorbent for Cr (VI) removal from aqueous solution in a batch system. Cr (VI) adsorption on Ti-PilB was highly affected by pH, where the optimum adsorption efficiency was recorded at pH 4. The adsorption kinetic investigation revealed that the adsorption process was reached the equilibrium state at 120 min. The adsorption kinetic model was predicted using the pseudo-first-order model and pseudo-second-order model. However, the adsorption data were best fitted with the pseudo-second-order model with the maximum adsorption capacity of 6.527 mg/g. The thermodynamic adsorption study of the adsorption data showed that the change of the Gibbs free energy (ΔG) value was negative, which mean that the adsorption process was spontaneous. Furthermore, the change of enthalpy value obtained to be positive indicated that the adsorption process was an endothermic nature.

Keywords: Bentonite, Adsorption, Hexavalent Chromium (Cr (VI)), Titanium, Pillared

INTRODUCTION

Chromium is one of the most used metals in various industries including stainless-steel manufacture, dye production, electroplating, paint manufacture, fertilizer, leather tanning, etc.[1,2] However, improper handling of wastewater from these various industries leads to the contamination of chromium in the environment, particularly in the aquatic ecosystem. Chromium contamination in the aquatic environment will be hazardous because chromium is a heavy metal that has bio-cumulative properties when entering the food chain. If the amount of chromium accumulation is high enough in a living thing, it will be able to endanger their lives[3].

In open environments, especially in aquatic ecosystems, chromium metal has many oxidizing states ranging from -2 to +6[4]. However, chromium with oxidation forms of +3 and +6 is the most common in nature. Both kinds of chromium metal have very different toxicity properties. Chromium in the form of +6 oxidation is much more toxic than chromium in the +3 oxidation form. in small amounts, Cr (III) is relatively safe and even highly needed by some living organisms in glucose metabolic mechanisms. In contrast, Cr (VI) has a very toxic nature even in trace amounts because it is so readily soluble in water that made it quickly spreads to the environment and accumulated in the food chain. Cr (VI) has carcinogenic properties to living organisms and even causing several diseases and even liver damage[5].

http://dx.doi.org/10.31788/RJC.2018.1133065

CrossMark

Hence, the Cr (VI) removal from wastewater is a necessary process before it could be discharged into the environment.

In the last few decades, various methods have been developed to treat waste and wastewater containing chromium metal before being discharged directly into the environment.[6–8] Several methods have been explored and tested in both laboratory and industrial scales, including chemical precipitation, membrane separation, electrochemical reduction, ion exchange, chemical and biological reduction, and solvent extraction.[9] Nevertheless, these methods have various limitations such as high operational costs, the generation of substances or other pollutant compounds, high energy consumption, need complicated technique and produce relatively low absorption efficiency[10].

Adsorption is mentioned as one of the most feasible and economical methods for dyes and heavy metal removal from wastewater due to its low operational cost and high in efficiency[11]. However, the removal capacity of the heavy metal in the adsorption process highly depends on the properties of the used adsorbent. The commercially available adsorbent materials, such as activated carbon[12, 13] and aluminium oxide[14], have been reported has high adsorption capability. But, the utilization of the commercial adsorbent material is limited due to its high cost and lack of recovery. Nowadays, various low-cost adsorbent materials have been widely developed and applied in chemical industry wastewater treatments, including agricultural waste and by-product, mining by-product, fruit peel, fly ash, and even clays and clay minerals.[15, 16]

Recently, the clay-based material has a vital role in wastewater treatment [17]. Bentonite is one of smectite clay which is mainly constructed of montmorillonite minerals. It has high potential to be utilized in broad fields, such as catalyst and adsorbent due to its high surface area, high thermal stability, and porous structured [18]. However, bentonite has one significant disadvantage, i.e. the lack of its permanent porosity. In high temperature, the structure of the bentonite layer collapse and no longer accessible for any surface process. To overcome this limitation, various methods have been developed, and the most suitable technique is by introducing the high stability ion-molecule into the interlayer region in order to create a high pore volume. Further, this method called as pillarization. Various pillaring different pillaring species have been tested, including organic cation, organometallic, metal oxide, and mixed metal oxide.

The metal oxide is the most evaluated pillaring species prepared by hydrolysis of the metal salt such as Al, Fe, Cr, Zr, and Ti. Compared with the others metal oxide pillared clay, the titanium pillared bentonite exhibits various advantage including high surface area and thermal stability, large pore size, high acidity and photo-catalytic capacity [19]. Hence, in this present study, the titanium pillared bentonite was prepared by varying the ratio of the Ti^{4+}/clay in order to investigate the effect of the amount of the titanium pillaring solution on the properties of the titanium-pillared bentonite properties. The pillared bentonite product was characterized and its capability as the adsorbent for Cr VI removal from aqueous solution was evaluated.

EXPERIMENTAL

Materials

Bentonite used as the host material used in this experiment was natural bentonite collected from a local deposit in Sarolangun District of Jambi Province, Indonesia. The preparation, purification, and characterization of the natural bentonite samples were described in our previous work [20]. All the others chemical used in this work such as hydrochloric acid (HCl), sodium hydroxide (NaOH), sulfuric acid (H_2SO_4), potassium dichromate ($K_2Cr_2O_7$), and 1,5 diphenylcarbazide were commercially available and use as received without further purification.

Synthesis of Ti-Pillared Bentonite

In this study, Ti-pillared bentonite was synthesized using titanium (VI) propoxide precursor. Tetravalent titanium pillar was prepared based on the previous work conducted by Tomul *et al.*[19] with slight modification. The titanium pillaring solution was prepared by slowly adding 12 mL of titanium propoxide into 27 mL HCl solution with a concentration of 6 M at room temperature followed by stirring for 3 hours. The solution then diluted with distilled water to obtain H^+ and Ti^{4+} concentration 1 M and 0.25 M, respectively. The pillaring solution then stirred for 6 hours at room temperature before it used further as the pillaring agent.

The Ti-pillared bentonite (Ti-PilB) was synthesized by adding the obtained Ti-pillaring solution drop wisely into bentonite suspension of 1% (by mass) with distilled water. Four Ti-PilB was prepared with different Ti/clay ratio, 1, 5, 10, and 15 mmol/g bentonite. The slurry solution then stirred for 24 hours at room temperature, and after finished the solid was washed for several times, separated by centrifugation and drying at 80 ºC for 16 hours. The obtained product then calcined at 400 ºC for 2 hours, and the results were labeled as Ti-PilB 1, Ti-PilB 5, Ti-PilB 10, and Ti-PilB 15, respectively.

Characterization

The natural bentonite and Ti-pillared bentonite samples were characterized by various techniques including X-Ray diffraction (XRD), Fourier Transform Infra-Red, and X-Ray Fluorescence. XRD analysis was conducted in order to analyze the structural properties of the smectite. The study was performed using a Rigaku Miniflex 600 X-ray diffractometer with CuK radiation at 30 kV and 10 mA. The measurement was recorded at 2 theta range about 3º to 60º with scanning speed 5º/min.

The functional group of the bentonite was analyzed by Shimadzu Prestige-21 FTIR spectrometer using KBr pellet method. The sample was scanned from wavenumber 400 to 4000 cm^{-1}. The chemical composition of the natural and Ti-pillared bentonite samples was characterized with X-ray fluorescence using XRF PANanalytical type Minipal 4 under air and helium condition.

Adsorbate Preparation

As much as 2.829 g of $K_2Cr_2O_7$ was dissolved in 1000 mL of distilled water in order to prepare the Cr (VI) stock solution with concentration 1000 mg/L. The standard solution of Cr (VI) was made by diluting the Cr (VI) stock solution into the desired concentration, 1 to 25 mg/L, with distilled water. The absorbance of the standard solution and the Cr (VI) concentration after the adsorption was determined using double beam spectrophotometer EMC LAB type EMC-61PC-UV using 1,5 diphenyl carbazide method at wavelength 540 nm.

Adsorption Studies

The adsorption capability of the Ti-PilB was tested by using Cr (VI) as the adsorbate. The whole adsorption experiments were carried out in a batch method. Typically, 50 mL of Cr (VI) solution was contacted with a certain amount of Ti-PilB adsorbent in a 100-mL canonical flask. The mixture than maintained in the horizontal shaker with the constant shaking speed of 250 rpm for predeterminate time. After finished, the mixture was separated using centrifugation at 4000 rpm for 10 minutes and the Cr (VI) concentration left was determined by double beam UV-Vis spectrophotometer using 1,5 diphenyl carbazide method.

Some operational parameter, including adsorbent dosage, initial pH of Cr (VI) solution, contact time, initial concentration of Cr (VI) solution, and adsorption temperature was investigated. The removal efficiency of Cr (VI) and the adsorption capacity of Ti-PilB were determined by equation (1) and equation (2), respectively.

$$\%Removal = \frac{(C_o - C_t)}{C_o} \cdot 100 \quad (1)$$

$$q_e = \frac{(C_o - C_e)}{m} \cdot V \quad (2)$$

$$q_t = \frac{(C_o - C_t)}{m} \cdot V \quad (3)$$

Where C_o is the initial concentration of Cr (VI) solution (mg/L), C_e is the Cr VI concentration at the equilibrium (mg/L), C_t is the Cr VI concentration after the adsorption process at any time t (mg/L), q_e is the adsorption capacity of Ti-PilB at equilibrium (mg/g), V is the volume of Cr (VI) solution (L), and m is the amount of Ti-PilB used (g).

RESULTS AND DISCUSSION

Ti-pillared Bentonite Characterization

X-ray diffraction analysis was subjected to the natural and Ti-pillared bentonite samples in order to study the change of structural properties and the degree of its crystallinity of the bentonite caused by the

insertion of the titanium pillar into the interlayer space. The results of the XRD powder pattern of natural bentonite and Ti-PilB are presented in Fig and $d_{(001)}$ reflection properties are tabulated in Table. The natural bentonite shows characteristic reflection peak of montmorillonite at 2θ around 6.33, 19.77, 34.96, and 34.96°. The others reflection peak at 2θ degree around 26.68 and 54.16° were recorded as the characteristic peak of quartz as impurities [21]. According to the Brag equation, the basal spacing of natural bentonite at 2θ = 6.3° correspond to the $d_{(001)}$ value 1.38 nm as the result of the presence of interlayer cation and the water molecule in the interlayer space of bentonite[22].

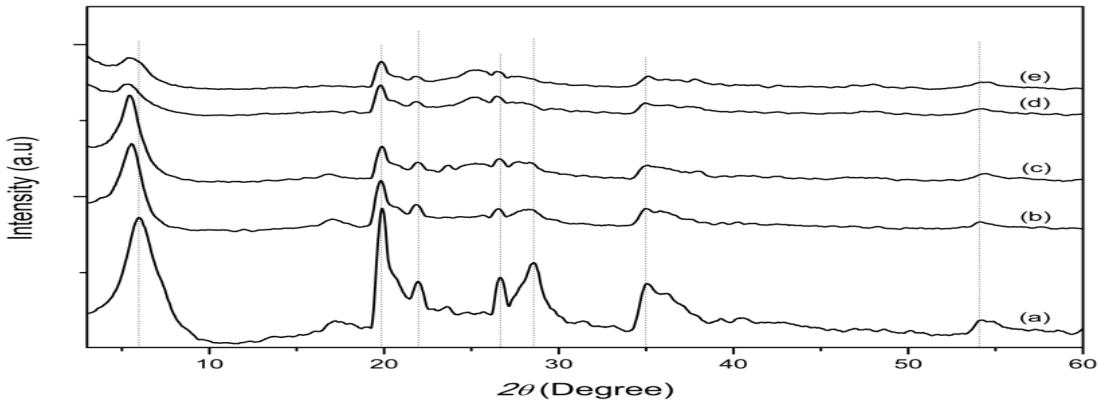

Fig.-1: XRD Pattern of Natural Bentonite (a), Ti-PilB 1(b), Ti-PilB 5 (c), Ti-PilB 10 (d), and Ti-PilB 15 (e)

After pillared with titanium, the intensity of the XRD pattern of natural bentonite decreased in all the characteristic reflection peak, particularly the d(001) peak at 2θ around 6°. This finding also reported by Caglar et al.,[23] which mean that the Ti-pillared bentonite product has a semi-crystalline structure. Moreover, the (001) characteristic peak at 6.39° was shifted to the lower degree correspond to the increase of the $d_{(001)}$ spacing as the effect of the titanium as the pillar species. In this case, the titanium pillaring solution has been transformed into the titanium oxide pillars after the calcination process. This finding is in agreement with the reported paper by previous researchers [24–26].

In more detail, the increase of the Ti^{4+} clay ratio to the 10 mmol/g causes the expansion of the basal spacing. However, the addition of Ti^{4+} clay ratio beyond 10 mmol/g causing the decrease in the basal spacing. As presented in Table, the basal spacing of Ti-PilB reached maximum 17.50 A at the Ti^{4+} clay ratio of 10 mmol/g. Hence, it was reasonable for us to conclude that 10 mmol/g is the maximum Ti^{4+}/clay ratio before the bentonite structure was delaminated. The interlayer opening due to the inclusion of the titanium pillar has been calculated by subtracting the $d_{(001)}$ spacing of the Ti-pillared bentonite with the thickness of the SiO_2-Al_2O_3-SiO_2 sheet, which value is 9.6 A and the result was presented in Table 1[23].

Table-1: Basal Spacing and Interlayer Opening of Natural Bentonite and Ti-Pillared Bentonite

Materials	2θ (°)	$d_{(001)}$(Å)	Interlayer Opening (Å)
Natural Bentonite	6.39	13.82	4.22
Ti-PilB 1	5.49	16.08	4.22
Ti-PilB 5	5.38	16.42	6.82
Ti-PilB 10	5.06	17.50	7.90
Ti-PilB 15	5.40	16.40	6.80

FTIR spectra of Ti-pillared bentonite was recorded at wavenumber 400 to 4000 cm^{-1} in order to investigate the change of the functional group in the bentonite framework after pillared by Ti^{4+}. The FTIR spectra of natural bentonite were also recorded for the comparison purpose. The FTIR spectra of Ti-pillared bentonite and natural bentonite are shown in Fig and the specific band of the bentonite framework was tabulated in Table. The FTIR spectra of natural bentonite represent the strong absorption band at 1010 cm^{-1} as the Si-O-Si stretching vibration. The characteristic band of the bentonite structure as the Al-OH-Al framework recorded at the 3441 cm^{-1} for stretching vibration and 900 cm^{-1} for bending vibration

[27]. The band at 3626 and 1639 cm^{-1} correspond to the characteristic band of H-O-H stretching and bending, respectively, of the inner water molecule, lied in the interlayer space of the bentonite. While the relatively weak band recorded at 416 and 516 cm^{-1} was recognized as the bending vibration of Si-O-Si and Si-O-Al, respectively [28].

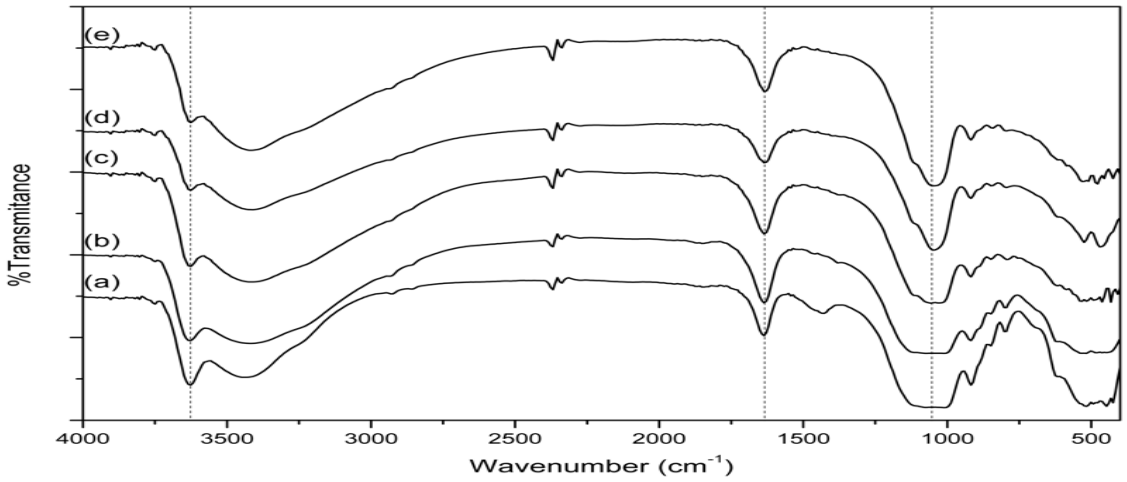

Fig.-2: FTIR Spectra of (a) Natural Bentonite and Ti-PilB 1(b), Ti-PilB 5 (c), Ti-PilB 10 (d), and Ti-PilB 15 (e)

Table-2: IR Absorption Properties of Natural and Ti-PilB

Materials	Wavenumber (cm^{-1})					
Natural Bentonite	416	516	1010	1635	3441	3626
Ti-PilB 1	447	516	1010	1635	3417	3626
Ti-PilB 5	462	532	1033	1635	3417	3626
Ti-PilB 10	470	524	1049	1635	3410	3626
Ti-PilB 15	478	532	1049	1635	3417	3626

The IR spectra of all Ti-pillared bentonite samples relatively correspond to the natural bentonite. This finding clarifies that the primary structure of the host bentonite was not changed during the pillaring process. As can be seen in Table-2 and Fig.-2, after the pillaring process, the characteristic band of the natural bentonite framework at 3441 cm^{-1} was shifted to the lower wavenumber followed by the peak width broadening. This finding is an indication that the pillaring process was causing an increase of the interlayer space content. This phenomenon occurred due to the replacement of the inorganic cation, which has relatively small size with the titanium pillars. In corresponding to the XRD analysis, the Ti-PilB 10 sample exhibit the highest shifting value, which is mean that Ti-PilB 10 has the highest interlayer content. Moreover, the intensity of specific -OH band of the water molecule recorded at 3626 cm^{-1} was decreased, which is signified that the interlayer cation in hydrated form was replaced by the titanium pillar in the metal oxide form during the pillaring process. The specific band of Si-O-Si at 1010 cm^{-1} also affected by the pillaring process. It was shifted to the higher wavenumber by increasing the amount of Ti^{4+} clay ratio. However, its peak intensity observed decrease after the pillaring process [29].

The chemical composition of the natural bentonite and Ti-pillared bentonite with various Ti^{4+} clay ratio is presented in Table. The results showed that all the samples have two main constituents, i.e. SiO_2 and Al_2O_3 since the main component of bentonite is montmorillonite mineral. The ratio of SiO_2:Al_2O_3 of the natural bentonite sample is 4.76. This finding is an indication that the natural bentonite has a significant amount of free silica[30].

The XRF analysis of the titanium pillared bentonite presented in Fi. The result showed that the fraction of TiO_2 increased gradually by increasing the Ti^{4+} clay ratio. On the other hand, the fraction of SiO_2 and Al_2O_3 decreased indicated that the TiO_2 had been successfully inserted in the interlayer structure of the bentonite. Furthermore, the fraction of the Al_2O_3 and SiO_2 slightly increased as the Ti^{4+} clay ratio increased beyond 10 mmol/g although the fraction of TiO_2 increased significantly. This finding informed

that the maximum of the interlayer space to be occupied by TiO_2 pillar reached with Ti^{4+} clay ratio of 10 mmol/g. Further increase of the Ti^{4+} clay ratio is causing the delamination of the bentonite structure with TiO_2. This result is an agreement with XRD and FTIR analysis. In this study, the mechanism of the TiO_2 pillarization on natural bentonite is described in Fig.

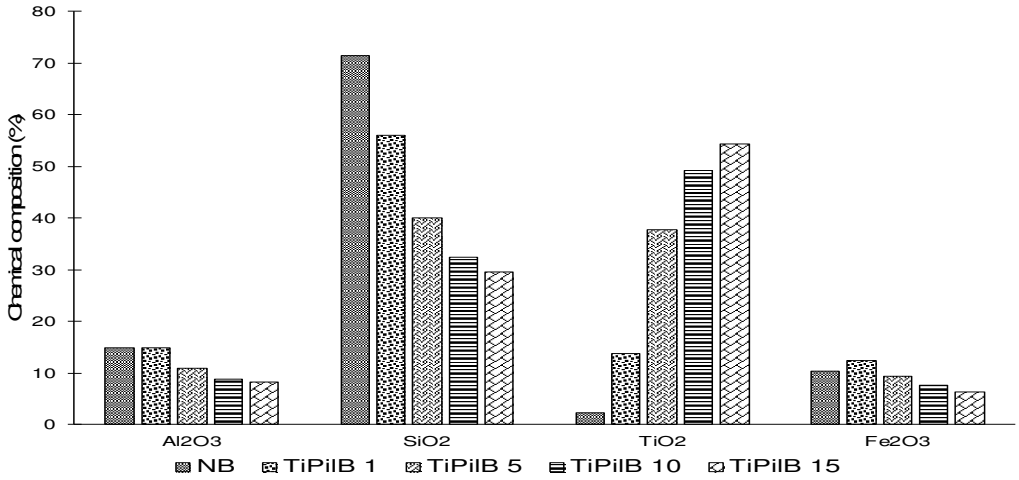

Fig.-3: Effect of Ti^{4+}/Clay Ratio on the Chemical Composition of Bentonite (NB) and Titanium Pillared Bentonite

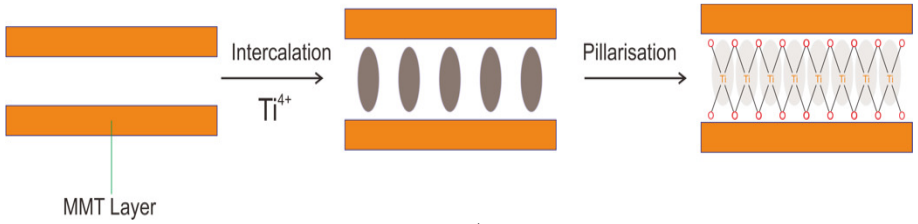

Fig.-4: Illustration Model of Ti^{4+} Intercalation on Bentonite

Adsorption Studies

Based on the result of the Ti-pillared bentonite characterization, the Ti-PilB 10 sample was utilized as the adsorbent for Cr (VI) removal conducted in this present study. In order to investigate the capability of the Ti-PilB on the adsorption of Cr (VI), various experimental parameters that affected the adsorption mechanism have been systematically evaluated, including adsorbent dosage, initial pH of the Cr (VI) solution, contact time, and temperature. The study of the adsorption kinetics was carried out by evaluating the pseudo-first-order and pseudo-second-order kinetic model. The thermodynamic parameter occurred during the adsorption process was also studied based on the experiment data at various temperature.

Table-3: Chemical Composition of Natural Bentonite (NB) and Ti-PilB

Composition (%)	NB	Ti-PilB 1	Ti-PilB 5	Ti-PilB 10	Ti-PilB 15
Al_2O_3	15	15	11	8.8	8.3
SiO_2	71.4	56	40.1	32.5	29.5
K_2O	0.13	0.52	0.38	0.27	0.26
CaO	0.35	2.08	0.73	0.58	0.42
TiO_2	2.24	13.7	37.7	49.22	54.33
V_2O_5	0.048	0.35	0	0	0
Cr_2O_3	0.048	0.007	0	0	0
Fe_2O_3	10.4	12.5	9.43	7.69	6.36
NiO	0	0.031	0	0	0
CuO	0.062	0.061	0.053	0.04	0.039
ZnO	0.02	0.088	0.061	0.099	0.079
Re_2O_7	0.09	0.06	0.09	0	0

Effect of Adsorbent Dosage

Study on the impact of the adsorbent dosage to the Cr (VI) adsorption efficiency was carried out by interacting a constant volume of 10 mg/L Cr (VI) solution with a various amount of the adsorbent (0.01 to 0.2 g). After finished, the remaining Cr (VI) concentration was determined with 1,5 diphenyl carbazide method using UV-Vis spectrophotometer. The effect of the adsorbent dosage on the Cr (VI) adsorption efficiency was presented in Fig. It is clear that the effectiveness of Cr (VI) adsorption was positively affected by the amount of the adsorbent used. By the increase of the adsorbent dosage, the adsorption efficiency gradually increased and reached a maximum at the adsorbent dosage 2 mg/L with 55 % of Cr (VI) adsorbed. This phenomenon affected by the increase in the availability of the active sites in the adsorbent surface. However, the further addition of the adsorbent amount has not enhanced the adsorption significantly and even tend to plateau. As mentioned by Chinoune et al.[31] this result might be caused by the aggregation of the active site of the adsorbent which is causing the decreasing of the total available active area.

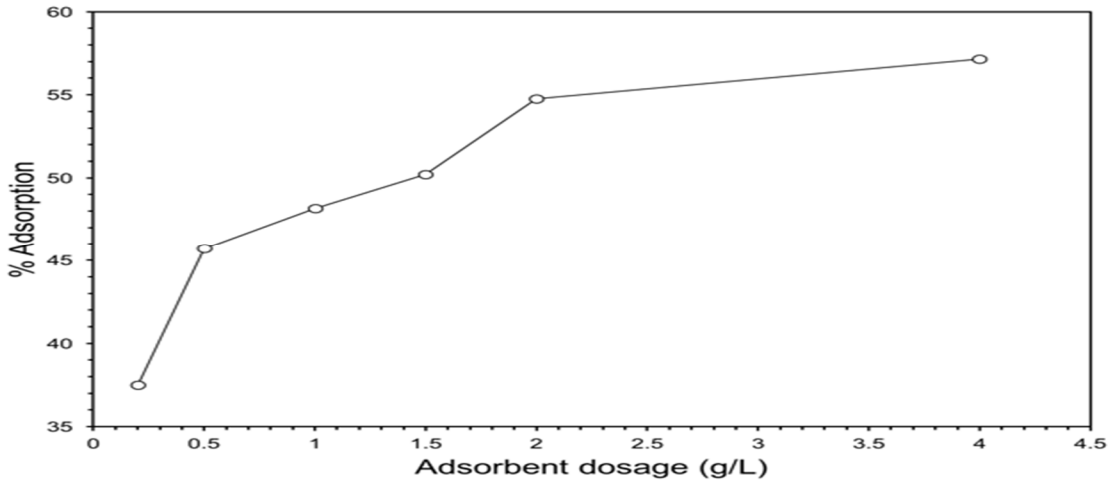

Fig.-5: Effect of the Adsorbent Dosage on the Adsorption Efficiency

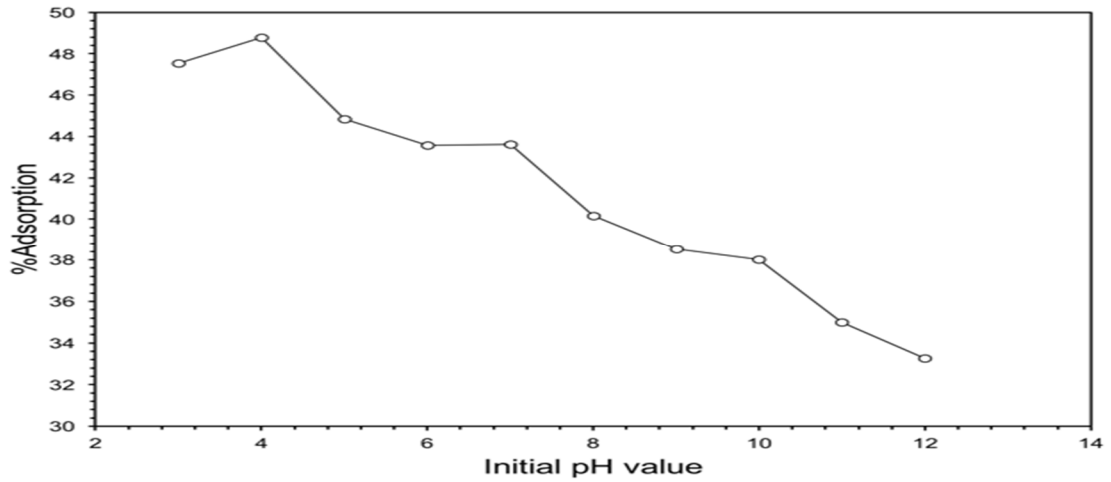

Fig.-6: Effect of Initial pH on the Performance of Cr (VI) Adsorption

Effect of Initial pH

Since the pH medium is profoundly affecting the speciation and degree of ionization of the Cr (VI) in the solution, it is crucial to further study the effect of pH medium on the efficiency of Cr (VI) adsorption on Ti-PilB. Hence, in this work, the adsorption process was evaluated over the various initial pH of the sorbate solution (ranging from 3 to 12). The result of the adsorption efficiency as the function of the initial pH medium is presented in Fig. The maximum adsorption efficiency was obtained at pH 4 and

gradually decreased by increasing the initial pH medium up to 12. This finding was an indication that the Cr (VI) adsorption on Ti-PilB favorably occurred in the acidic condition. In low pH value (pH< 4), based on the solubility equilibrium, the hexavalent chromium exists in $HCrO^{4-}$ form dominantly. Moreover, the surface of the bentonite was positively charged in the acidic medium. Hence, the capability of Cr (VI) to be adsorbed on the surface of the adsorbent enhanced in the acidic pH medium.

Adsorption Kinetic

The adsorption kinetic study was employed in order to predict the adsorption mechanism and the rate-limiting steps involved in the adsorption rate investigation. The kinetic study was carried out in batch adsorption experiments with varying the contact time. The result in the form of the adsorption efficiency as the effect of contact time is shown in Figure-7. It was found that the adsorption equilibrium was reached within 120 min. However, it observed that at the beginning, the adsorption process was conducted rapidly, and after 10 minutes the adsorption process was slowed down until achieving its equilibrium condition. This finding describes that at the initial adsorption stage, the active site of the adsorbent has high affinity and the number of the adsorbent active site was available. By increasing the contact time, the available adsorption site limited and the Cr (VI) uptake was gradually decreased and eventually reached the equilibrium condition.

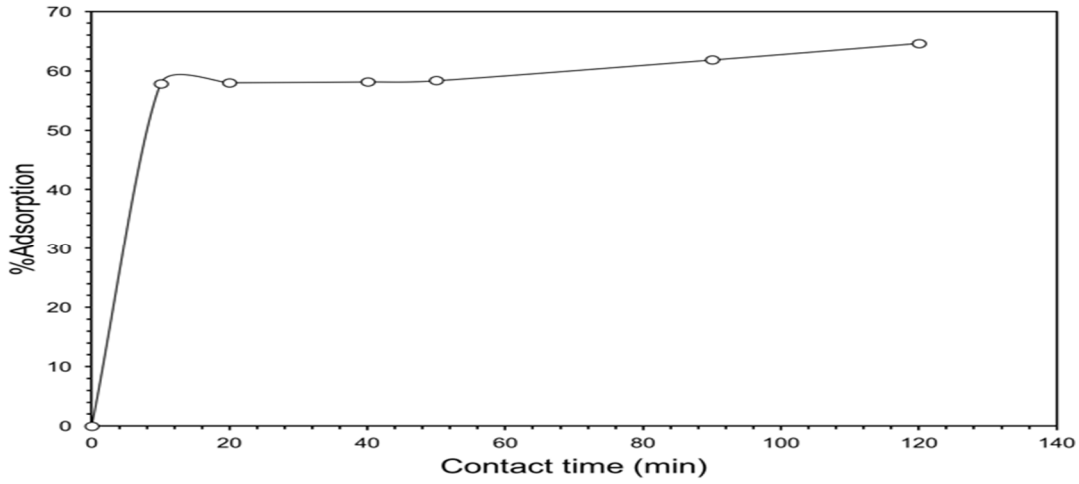

Fig.-7: Effect of Contact Time on Cr (VI) Adsorption

Table-4: Adsorption Kinetics Parameter of Cr (VI) on Ti-PilB According to the P-FO and P-SO Kinetics Model

Kinetic Model				
P-FO	k_1 (min^{-1})	q_e, theo (mg/g)	q_e, exp (mg/g)	R^2
	0.011	0.876	6.464	0.803
P-SO	k_2 (g/mg min)	q_e (mg/g)	h (mg/g min)	R^2
	0.044	6.527	1.893	0.997

A further study on the adsorption mechanism was conducted by employing the two most studied adsorption kinetic model, the pseudo-first-order P-FO and pseudo-second-order P-SO model, to the experimental result. P-FO model was developed on the assumption that the mechanism involved in the adsorption process was controlled by the mass transfer and the diffusion of Cr (VI) ion in the Ti-PilB active site. The P-SO model was developed based on the assumption that the adsorption mechanism was controlled by the chemisorption which is the rate-limiting step during the adsorption process occurred. The linearized form of the P-FO and P-SO model are presented in the equation (4), and equation (5), respectively.

$$\log(q_e - q_t) = \log q_e - \frac{k_1}{2.303} \cdot t \quad (4)$$

$$\frac{t}{q_t} = \frac{1}{k_2 q_e^2} + \frac{t}{q_e} \quad (5)$$

$$h = k_2 q_e^2 \quad (6)$$

Where q_t and q_e are the amounts of the Cr (VI) ion adsorbed per unit mass of adsorbent at any time t, and at equilibrium, respectively (mg/g). k_1 and k_2 are the rate constant of the P-FO model (min^{-1}) and P-SO model ($mg^{-1}\ h^{-1}$), respectively.

The kinetic adsorption parameters, based on both P-FO and P-SO kinetic model, were determined from the slope and intercept of the linear plot of $\log(q_e - q_t)$ against t from the P-FO equation model and plot of t/qt versus t from the P-SO equation model. The initial of the adsorption rate (h) was determined based on eqn.-6, related to the P-SO kinetic model. The linear fit for P-FO and P-SO models was presented in Fig, and the kinetic parameters including rate constant and the equilibrium adsorption capacity were tabulated in Table.

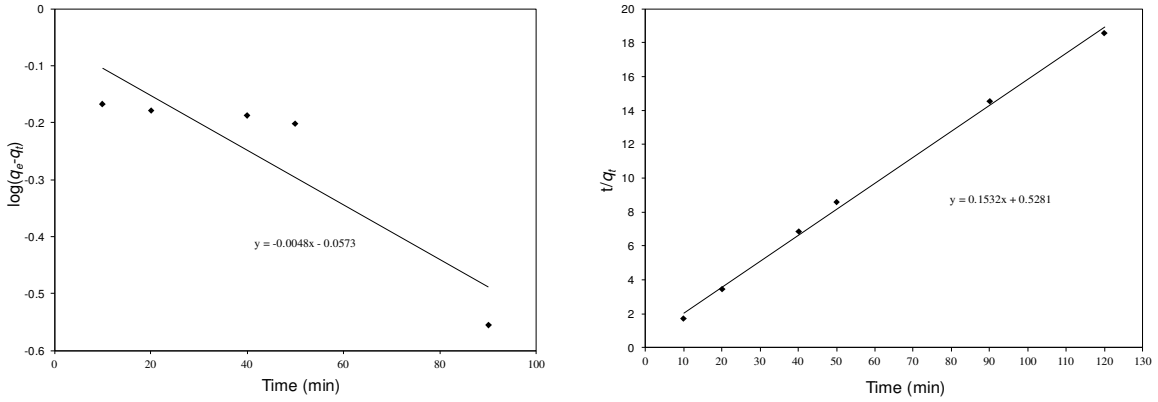

(a) (b)

Fig.-8: Plot of Adsorption Kinetics Model for Cr (VI) Adsorption

The conformity of the of the used kinetic model to the experimental result was investigated based on the value of the regression coefficient R^2. As listed in Table, the R^2 value of the P-FO model was less than 0.99 indicating that the model was not sufficient for modeling the experiment result. Meanwhile, the P-SO model emerged as a good regression coefficient with a magnitude value more than 0.99. This finding describes that the adsorption kinetics of Cr (VI) on Ti-PilB was preferably described by using the P-SO kinetic model.

Adsorption Thermodynamic

The thermodynamic parameters of the Cr (VI) adsorption on the Ti-PilB was investigated in order to evaluate the influence of the temperature on the adsorption process. The experiment was carried out at various temperature, 303 to 333 K, with constant contact time and initial Cr (VI) solution concentration. The constant of the equilibrium thermodynamic K_d as the constant of the Cr (VI) distribution on the liquid and solid at equilibrium could be calculated using the following equation.

$$K_D = \frac{q_e}{C_e} \tag{7}$$

$$\ln K_d = \frac{-\Delta H}{RT} + \frac{\Delta S}{R} \tag{8}$$

$$\Delta G = \Delta H - T\Delta S \tag{9}$$

Where ΔG^o, ΔH^o, and ΔS^o are the change of the Gibbs free energy kJ/mol, the change of the enthalpy kJ/mol, and the change of the of the entropy kJ/mol K, respectively. While R and T are the gas constant 8.314 J/mol K and thermodynamic temperature, respectively. The Van't Hoff equation as presented in equation (8) and (9) was calculated for determining the thermodynamic parameter including ΔH^o, ΔS^o, and ΔG^o by plotting the distribution constant K_d against 1/T at the different temperature used during the experiment.

The plot of K_D as the function of 1/T based on the result of the experiment was presented in Fig. The plot produced a straight line with correlation coefficient R^2 value 0.9902. The thermodynamic parameter of ΔH^o and ΔS^o based on the Van's Hoff equation was presented in Table. The results showed that by increasing the adsorption temperature from 303 K to 333 K, the change of Gibbs free energy decreased

from -0.224 to -3.098 kJ/mol. This result indicated that the adsorption process was favourable occurred in high temperature [32]. The positive value of the change of the adsorption enthalpy revealed that the adsorption nature was endothermic. Since the physical adsorption process occurred in the range of enthalpy change -20 to 40 kJ/mol and chemical adsorption occurred in the range of -400 to 80 kJ/mol, the value of the enthalpy changes of 28.79 kJ/mol informed that the adsorption process was a physical adsorption. Moreover, the positive value of the entropy changes revealed that the randomness of the adsorption process increases irregularly [32].

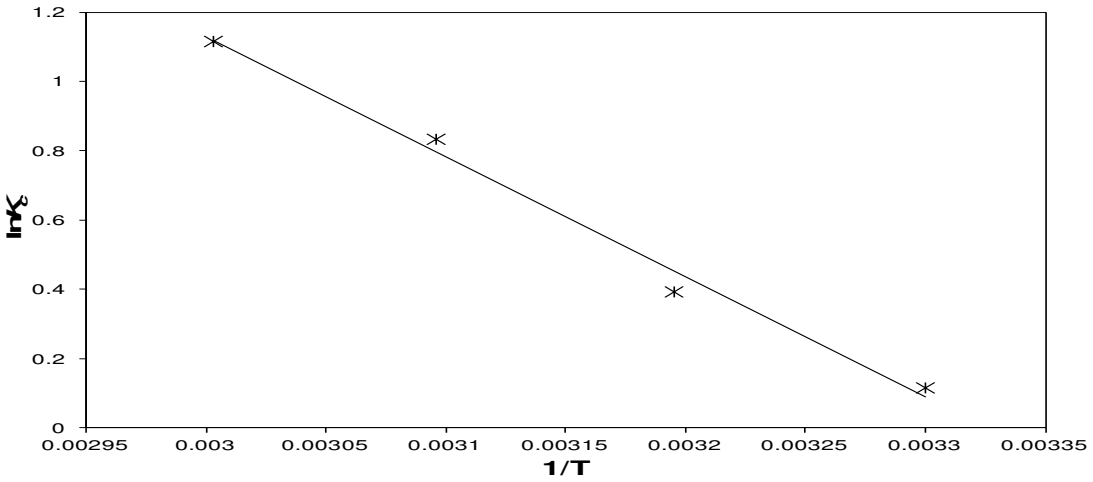

Fig.-9: Plot of $ln\ K_d$ Versus 1/T

Table-5: Thermodynamic Parameters for Cr (VI) Adsorption

ΔS (J/mol)	ΔH (kJ/mol)	Temperature (K)	ΔG (kJ/mol)
95.78	28.79	303	-0.224
-	-	313	-1.182
-	-	323	-2.140
-	-	333	-3.098

CONCLUSION

The titanium-pillared bentonite prepared form the natural bentonite with various Ti^{4+}/clay ratio has been synthesized. The results show that the basal spacing of the Ti-pillared bentonite increased gradually by increasing the Ti^{4+}/clay ratio. Furthermore, Ti^{4+}/clay ratio 10 mmol/g was as the maximum ratio before the bentonite framework was delaminated. The utilization of the Titanium pillared bentonite for Cr (VI) removal showed that the adsorption process was profoundly affected by the pH of the solution. The adsorption kinetic investigation revealed that the adsorption process followed the pseudo-second-order model with adsorption capacity at equilibrium reached 6.527 mg/g. The study on adsorption thermodynamic showed that the adsorption process was spontaneous with endothermic nature.

ACKNOWLEDGMENT

The author profoundly thanks to Ministry of Research, Technology and Higher Education (KEMENRISTEKDIKTI) of Republic Indonesia for the financial supporting this research through PMDSU (Program Magister Menuju Doktor Untuk Sarjana Unggul) grant with contract number 326/SP2H/LT/ DRPM/IX/2016 and 468/UN9.3.1/LT/2017.

REFERENCES

1. H. Chen, J. Dou, and H. Xu, *Appl. Surf. Sci.*, **425**, 728 (2017), DOI: 10.1016/j.apsusc.2017.07.053.
2. A. Kumar and H. M. Jena, *Process Saf. Environ. Prot.*, **109**, 63 (2017), **DOI:** 10.1016/j.psep.2017.03.032.
3. K. Zhang, H. Li, X. Xu, and H. Yu, *Microporous Mesoporous Mater.*, **255**, 7 (2018), **DOI:** 10.1016/j.micromeso.2017.07.037.

4. Q. Liang, J. Geng, H. Luo, W. Fang, and Y. Yin, *J. Mol. Liq.*, **248**, 767 (2017), **DOI:** 10.1016/j.molliq.2017.10.114.
5. G. Bayramou glu, G. Çelik, E. Yalçın, M. Yılmaz, and M. Y. Arıca, *J. Hazard. Mater.*, **119**, 219 (2005), DOI: 10.1016/j.jhazmat.2004.12.022.
6. X. Liang, X. Fan, R. Li, S. Li, S. Shen, and D. Hu, *Bioresour. Technol.*, **250**, 178 (2018), **DOI:** 10.1016/j.biortech.2017.10.071.
7. X. Jin, Y. Liu, J. Tan, G. Owens, and Z. Chen, *J. Clean. Prod.*, **176**, 929 (2018), **DOI:** 10.1016/j.jclepro.2017.12.026.
8. L.-L. Li, X.-Q. Feng, R.-P. Han, S.-Q. Zang, and G. Yang, *J. Hazard. Mater.*, **321**, 622 (2017), **DOI:** 10.1016/j.jhazmat.2016.09.029.
9. B. Anup Nikhil, S. Ramesh, S. Dhanasekar, and J. S. Sudarsan, *Rasayan J. Chem.*, **10**, 1114 (2017), DOI: 10.7324/RJC.2017.1041729.
10. G. Wang, Y. Hua, X. Su, S. Komarneni, S. Ma, and Y. Wang, *Appl. Clay Sci.*, **124–125**, 111 (2016), DOI: 10.1016/j.clay.2016.02.008.
11. Y. Bayrak, Y. Yesiloglu, and U. Gecgel, *Microporous Mesoporous Mater.*, **91**, 107 (2006), **DOI:** 10.1016/j.micromeso.2005.11.010.
12. O. Kazak, Y. R. Eker, H. Bingol, and A. Tor, *Bioresour. Technol.*, **241**, 1077 (2017), **DOI:** 10.1016/j.biortech.2017.06.062.
13. N. Gopal and M. Asaithambi, *Rasayan J. Chem.*, **8**, 279 (2015).
14. M. A. Mahmoud, *Beni-Suef Univ. J. Basic Appl. Sci.*, **4**, 142 (2015), **DOI:** 10.1016/j.bjbas.2015.05.008.
15. P. Pranoto, C. Purnawan, and T. Utami, *Rasayan J. Chem.*, **11**, 23 (2018), **DOI:** 10.7324/RJC.2018.1111939.
16. T. Taher, D. Rohendi, R. Mohadi, and A. Lesbani, *Chiang Mai J. Sci.*, **45**, 1770 (2018).
17. Z. Huang *et al.*, *Mater. Chem. Phys.*, **202**, 266 (2017), **DOI:** 10.1016/J.MATCHEMPHYS.2017.09.028.
18. F. Tomul, *Appl. Clay Sci.*, **120**, 121 (2016), DOI: 10.1016/j.clay.2015.11.007.
19. F. Tomul, F. Turgut Basoglu, and H. Canbay, *Appl. Surf. Sci.*, **360**, 579 (2016), **DOI:** 10.1016/j.apsusc.2015.10.228.
20. T. Taher, R. Mohadi, D. Rohendi, and A. Lesbani, in *International Conference on Chemistry Chemical Process and Engineering*, **1823**, (2017), **DOI:** 10.1063/1.4978101.
21. R. Fabryanty *et al.*, *J. Environ. Chem. Eng.*, **5**, 5677 (2017), **DOI:** 10.1016/j.jece.2017.10.057.
22. C.-C. Wang, X.-D. Du, J. Li, X.-X. Guo, P. Wang, and J. Zhang, *Appl. Catal. B Environ.*, **193**, 198 (2016), **DOI:** 10.1016/j.apcatb.2016.04.030.
23. B. Caglar *et al.*, *J. Mol. Struct.*, **1089**, 59 (2015), **DOI:** 10.1016/j.molstruc.2015.02.034.
24. C. Y. Cao, L. K. Meng, and Y. H. Zhao, *Toxicol. Environ. Chem.*, **95**, 747 (2013), **DOI:** 10.1080/02772248.2013.806512.
25. P. Kumararaja, K. M. Manjaiah, S. C. Datta, and B. Sarkar, *Appl. Clay Sci.*, **137**, 115 (2017), **DOI:** 10.1016/j.clay.2016.12.017.
26. F. Tomul, *Chem. Eng. J.*, **185–186**, 380 (2012), **DOI:** 10.1016/j.cej.2012.01.094.
27. M. F. Hou, C. X. Ma, W. De Zhang, X. Y. Tang, Y. N. Fan, and H. F. Wan, *J. Hazard. Mater.*, **186**, 1118 (2011), **DOI:** 10.1016/j.jhazmat.2010.11.110.
28. A. Tabak, B. Afsin, B. Caglar, and E. Koksal, *J. Colloid Interface Sci.*, **313**, 5 (2007), **DOI:** 10.1016/j.jcis.2007.02.086.
29. F. T. Basoglu and S. Balci, *J. Mol. Struct.*, **1106**, 382 (2016), **DOI:** 10.1016/j.molstruc.2015.10.072.
30. D. Hank, Z. Azi, S. Ait Hocine, O. Chaalal, and A. Hellal, *J. Ind. Eng. Chem.*, **20**, 2256 (2014), **DOI:** 10.1016/j.jiec.2013.09.058.
31. K. Chinoune, K. Bentaleb, Z. Bouberka, A. Nadim, and U. Maschke, *Appl. Clay Sci.*, **123**, 64 (2016), **DOI:** 10.1016/j.clay.2016.01.006.
32. W. Wang, B. Zheng, Z. Deng, Z. Feng, and L. Fu, *Chem. Eng. J.*, **214**, 343 (2013), **DOI:** 10.1016/j.cej.2012.10.070.

[RJC-3065/2018]